

Effect of shape anisotropy on the phase diagram of the Gay-Berne fluid

Pankaj Mishra and Jokhan Ram

Department of Physics, Banaras Hindu University, Varanasi-221 005, India

(Dated: November 8, 2018)

Abstract

We have used the density functional theory to study the effect of molecular elongation on the isotropic-nematic, isotropic-smectic A and nematic-smectic A phase transitions of a fluid of molecules interacting via the Gay-Berne intermolecular potential. We have considered a range of length-to-width parameter $3.0 \leq x_0 \leq 4.0$ in steps of 0.2 at different densities and temperatures. Pair correlation functions needed as input information in density functional theory are calculated using the Percus-Yevick integral equation theory. Within the small range of elongation, the phase diagram shows significant changes. The fluid at low temperature is found to freeze directly from isotropic to smectic A phase for all the values of x_0 considered by us on increasing the density while nematic phase stabilizes in between isotropic and smectic A phases only at high temperatures and densities. Both isotropic-nematic and nematic-smectic A transition density and pressure are found to decrease as we increase x_0 . The phase diagram obtained is compared with computer simulation result of the same model potential and is found to be in good qualitative agreement.

PACS numbers: 64.70.Md, 61.30.Cz, 61.30.Dk

I. INTRODUCTION

Liquid crystal phases which are formed by highly anisotropic complex organic molecules have symmetries intermediate between those of isotropic liquid and crystals. The simplest of the liquid crystal phases that find application in many electro-optic devices are nematic (N) and smectic A (Sm A) ones. In the nematic phase, molecules tend to align along a preferred direction called director, breaking the rotational invariance of isotropic liquid (I) but not the translational invariance. Partial breakdown of translational invariance along with breaking of rotational invariance introduces smectic phases where molecules are essentially confined in layers. In Sm A phase molecules are aligned perpendicular to layers with no intralayer or interlayer correlation in positions of the center of mass of the molecules. The properties and relative stability of these phases are extremely sensitive to the details of molecular structure and the true nature of intermolecular interaction potential[1]. Therefore, it is of interest for either computer simulation or theory to study the effect of molecular shape anisotropy and intermolecular potential on the liquid crystalline phase behaviour and properties.

Because of the complex structure of the mesogenic molecules it is very difficult to know the exact nature of the interaction potential as a function of intermolecular separation and orientation. Therefore, modeling of the intermolecular potential only with more physically relevant features become inevitable. The pair interaction potential model proposed by Gay and Berne (GB)[2] is one such model that includes anisotropic attractive interactions along with short range repulsive interactions. It has now become a standard model to study liquid crystalline phases and has been widely used in the investigation of various phenomena through computer simulation[3-13] and also theoretically[14-18].

In the Gay-Berne (GB) pair potential model, the molecules are considered as ellipsoids of revolution about the principal axis of the molecule. The interaction potential between two such ellipsoidal molecules i and j depends on direction $\hat{\mathbf{r}}_{ij}$ and on the magnitude of center-center vector $\mathbf{r}_{ij} = \mathbf{r}_i - \mathbf{r}_j$ and upon molecular axis vectors $\hat{\mathbf{e}}_i$ and $\hat{\mathbf{e}}_j$.

The GB potential is expressed as

$$u(\hat{\mathbf{e}}_i, \hat{\mathbf{e}}_j, \mathbf{r}_{ij}) = 4\epsilon_0 \epsilon^\nu(\hat{\mathbf{e}}_i, \hat{\mathbf{e}}_j) \epsilon'^\mu(\hat{\mathbf{e}}_i, \hat{\mathbf{e}}_j, \hat{\mathbf{r}}_{ij}) \times \left[\left(\frac{r_{ij} - \sigma(\hat{\mathbf{e}}_i, \hat{\mathbf{e}}_j, \hat{\mathbf{r}}_{ij}) + \sigma_0}{\sigma_0} \right)^{-12} - \left(\frac{r_{ij} - \sigma(\hat{\mathbf{e}}_i, \hat{\mathbf{e}}_j, \hat{\mathbf{r}}_{ij}) + \sigma_0}{\sigma_0} \right)^{-6} \right] \quad (1.1)$$

The angle dependent range parameters σ and strength functions ϵ are given by

$$\sigma(\hat{\mathbf{e}}_i, \hat{\mathbf{e}}_j, \hat{\mathbf{r}}_{ij}) = \sigma_0 \left[1 - \chi \left(\frac{(\hat{\mathbf{e}}_i \cdot \hat{\mathbf{r}}_{ij})^2 + (\hat{\mathbf{e}}_j \cdot \hat{\mathbf{r}}_{ij})^2}{1 - \chi^2(\hat{\mathbf{e}}_i \cdot \hat{\mathbf{e}}_j)^2} - \frac{2\chi(\hat{\mathbf{e}}_i \cdot \hat{\mathbf{r}}_{ij})(\hat{\mathbf{e}}_j \cdot \hat{\mathbf{r}}_{ij})(\hat{\mathbf{e}}_i \cdot \hat{\mathbf{e}}_j)}{1 - \chi^2(\hat{\mathbf{e}}_i \cdot \hat{\mathbf{e}}_j)^2} \right) \right]^{-\frac{1}{2}} \quad (1.2)$$

$$\epsilon(\hat{\mathbf{e}}_i, \hat{\mathbf{e}}_j) = [1 - \chi^2(\hat{\mathbf{e}}_i \cdot \hat{\mathbf{e}}_j)^2]^{-\frac{1}{2}} \quad (1.3)$$

$$\epsilon'(\hat{\mathbf{e}}_i, \hat{\mathbf{e}}_j, \hat{\mathbf{r}}_{ij}) = \left[1 - \chi' \left(\frac{(\hat{\mathbf{e}}_i \cdot \hat{\mathbf{r}}_{ij})^2 + (\hat{\mathbf{e}}_j \cdot \hat{\mathbf{r}}_{ij})^2}{1 - \chi'^2(\hat{\mathbf{e}}_i \cdot \hat{\mathbf{e}}_j)^2} - \frac{2\chi'(\hat{\mathbf{e}}_i \cdot \hat{\mathbf{r}}_{ij})(\hat{\mathbf{e}}_j \cdot \hat{\mathbf{r}}_{ij})(\hat{\mathbf{e}}_i \cdot \hat{\mathbf{e}}_j)}{1 - \chi'^2(\hat{\mathbf{e}}_i \cdot \hat{\mathbf{e}}_j)^2} \right) \right] \quad (1.4)$$

where σ_0 is the smallest molecular diameter and ϵ_0 is the energy scaling parameter equal to the well depth for the cross configuration ($\hat{\mathbf{e}}_i \cdot \hat{\mathbf{e}}_j = \hat{\mathbf{r}}_{ij} \cdot \hat{\mathbf{e}}_i = \hat{\mathbf{r}}_{ij} \cdot \hat{\mathbf{e}}_j = 0$). The parameter χ is a measure of shape anisotropy defined as $\chi = (x_0^2 - 1)/(x_0^2 + 1)$ with x_0 being the length-to-width ratio of the molecule. Though x_0 measures the anisotropy of the repulsive core, it also determines the difference in the depth of the attractive well between the side-by-side and the cross configurations. The parameter χ' determines the energy anisotropy defined as $\chi' = (k'^{1/\mu} - 1)/(k'^{1/\mu} + 1)$, where k' is the well-depth ratio for side-by-side and end-to-end configuration. The powers μ and ν entering in the energy functions are adjustable exponents determining the strength of interaction.

The GB model contains four parameters (x_0, k', μ, ν) that determine the anisotropy in the repulsive and attractive forces in addition to two parameters (σ_0, ϵ_0) that scale the distance and energy, respectively. The choices for the values of these parameters are in no way unique and they can be varied to yield a wide range of anisotropic potential[3]. The most

commonly used values of these parameters in the literature are $x_0 = 3.0, k' = 5, \mu = 2, \nu = 1$. In their molecular dynamic simulation study for this set of parameters de Miguel *etal*[4, 5] found three phases, namely, isotropic, nematic and smectic B. No Sm A phase was found to be stable. However, existence of Sm A phase has been reported for the set of parameters $x_0 = 3.0, k' = 5, \mu = 1, \nu = 2$ [6]. Recently the effect that changes in the well depth parameter k' [7, 15] and molecular elongation x_0 [8, 9, 17] have upon the overall phase behaviour of the system has been investigated. It was found that with the increase in k' the Sm B phase is favored at low density while the nematic phase becomes increasingly stable at lower temperature as k' is decreased. The variation of molecular elongation parameter x_0 has been found to have a significant effect. An island of Sm A is found to appear in the phase diagram for elongations above $x_0 = 3.0$ [9]. The range of Sm A extends to both higher and lower temperatures as x_0 is increased. Also the isotropic-nematic (I-N) transition is seen to move to lower density (and pressure) at a given temperature with the increase in x_0 .

In this paper we use the density functional theory (DFT) to study the effect of the variation of the length-to-breadth ratio x_0 on the freezing transitions and freezing parameters for the I-N, I-Sm A and N-Sm A transition for a system of molecule interacting via the Gay-Berne pair potential. The value of x_0 has been varied from 3.0 to 4.0 in steps of 0.2, keeping other parameters fixed at $k' = 5, \mu = 2$ and $\nu = 1$. Pair correlation functions needed as input information in the DFT have been calculated using the Percus-Yevick (PY) integral equation theory. The paper is organized as follows: In section II we describe in brief the density- functional formalism used to locate the freezing transitions and freezing parameters. We discuss our results and compare with the available simulation results in section III and finally conclude our discussion in section IV.

II. FUNDAMENTALS OF THE DENSITY-FUNCTIONAL THEORY OF FREEZING

The density functional theory (DFT) directly links the bulk phase behaviour of a fluid with its molecular properties. In DFT, the equilibrium density profile of a non uniform anisotropic liquid can be determined as the one that minimizes the grand thermodynamic potential W regarded as a functional of the single-particle density function $\rho(\mathbf{r}, \mathbf{\Omega})$ at point \mathbf{r} and orientation $\mathbf{\Omega}$.

The grand thermodynamic potential has the general form

$$-W = \beta A - \beta \mu_c \int d\mathbf{x} \rho(\mathbf{x}) \quad (2.1)$$

where A is the Helmholtz free energy, μ_c the chemical potential and $\rho(\mathbf{x})$ is a singlet distribution function, to locate the transition.

The above mentioned minimum property of the grand thermodynamic potential follows from the variational inequality

$$W[\rho_{eq}] \leq W[\rho] \quad (2.2)$$

which is valid for a fixed temperature and chemical potential, where ρ_{eq} is the equilibrium density profile.

It is convenient to subtract the isotropic fluid thermodynamic potential from W and write it as [19]

$$\Delta W = W - W_f = \Delta W_1 + \Delta W_2 \quad (2.3)$$

with

$$\frac{\Delta W_1}{N} = \frac{1}{\rho_f V} \int d\mathbf{r} d\mathbf{\Omega} \left\{ \rho(\mathbf{r}, \mathbf{\Omega}) \ln \left[\frac{\rho(\mathbf{r}, \mathbf{\Omega})}{\rho_f} \right] - \Delta \rho(\mathbf{r}, \mathbf{\Omega}) \right\} \quad (2.4)$$

and

$$\frac{\Delta W_2}{N} = -\frac{1}{2\rho_f} \int d\mathbf{r}_{12} d\mathbf{\Omega}_1 d\mathbf{\Omega}_2 \Delta \rho(\mathbf{r}_1, \mathbf{\Omega}_1) \times c(\mathbf{r}_{12}, \mathbf{\Omega}_1, \mathbf{\Omega}_2) \Delta \rho(\mathbf{r}_2, \mathbf{\Omega}_2) \quad (2.5)$$

Here $\Delta \rho(\mathbf{r}, \mathbf{\Omega}) = \rho(\mathbf{r}, \mathbf{\Omega}) - \rho_f$, where ρ_f is the density of the coexisting liquid.

The order parameter equation is obtained by minimizing ΔW with respect to the arbitrary variation in the ordered phase density subject to a constraint that corresponds to some specific feature of the ordered phase. This leads to

$$\ln \frac{\rho(\mathbf{r}_1, \mathbf{\Omega}_1)}{\rho_f} = \lambda_L + \int d\mathbf{r}_2 d\mathbf{\Omega}_2 c(\mathbf{r}_{12}, \mathbf{\Omega}_1, \mathbf{\Omega}_2; \rho_f) \Delta \rho(\mathbf{r}_2, \mathbf{\Omega}_2) \quad (2.6)$$

where λ_L is Lagrange multiplier. Equation(10) is solved by expanding the singlet distribution $\rho(\mathbf{r}, \mathbf{\Omega})$ in terms of the order parameters that characterize the ordered structures using the Fourier series and Wigner rotation matrices . Thus

$$\rho(\mathbf{r}, \mathbf{\Omega}) = \rho_0 \sum_q \sum_{lmn} Q_{lmn}(G_q) \exp(i\mathbf{G}_q \cdot \mathbf{r}) D_{mn}^l(\mathbf{\Omega}) \quad (2.7)$$

where the expansion coefficients

$$Q_{lmn}(G_q) = \frac{2l+1}{N} \int d\mathbf{r} \int d\mathbf{\Omega} \rho(\mathbf{r}, \mathbf{\Omega}) \times \exp(-i\mathbf{G}_q \cdot \mathbf{r}) D_{mn}^{*l}(\mathbf{\Omega}) \quad (2.8)$$

are the order parameters, \mathbf{G}_q the reciprocal lattice vectors, ρ_0 the mean number density of the ordered phase and $D_{mn}^{*l}(\mathbf{\Omega})$ the generalized spherical harmonics or Wigner rotation matrices. Note that for a uniaxial system consisting of cylindrically symmetric molecules $m = n = 0$ and, therefore, one has

$$\rho(\mathbf{r}, \mathbf{\Omega}) = \rho_0 \sum_l \sum_q Q_{lq} \exp(i\mathbf{G}_q \cdot \mathbf{r}) P_l(\cos \theta) \quad (2.9)$$

and

$$Q_{lq} = \frac{2l+1}{N} \int d\mathbf{r} \int d\mathbf{\Omega} \rho(\mathbf{r}, \mathbf{\Omega}) \exp(-i\mathbf{G}_q \cdot \mathbf{r}) P_l(\cos \theta) \quad (2.10)$$

where $P_l(\cos \theta)$ is the Legendre polynomial of degree l and θ is the angle between the cylindrical axis of a molecule and the director.

In the present calculation we consider two orientational order parameters

$$\bar{P}_l = \frac{Q_{l0}}{2l+1} = \langle P_l(\cos \theta) \rangle \quad (2.11)$$

with $l=2$ and 4 , one order parameter corresponding to positional order along Z axis,

$$\bar{\mu} = Q_{00}(G_z) = \langle \cos(\frac{2\pi}{d}z) \rangle \quad (2.12)$$

(d , being the layer spacing) and one mixed order parameter that measures the coupling between the positional and orientational ordering and is defined as,

$$\tau = \frac{1}{5} Q_{20}(G_z) = \langle \cos(\frac{2\pi}{d}z) P_2(\cos \theta) \rangle \quad (2.13)$$

The angular bracket in above equations indicate the ensemble average.

The following order parameter equations are obtained by using Eqs.(13) and (17) [18];

$$\bar{P}_l = \frac{1}{2d} \int_0^d dz_1 \int_0^\pi \sin \theta_1 d\theta_1 P_l(\cos \theta_1) \exp[sum] \quad (2.14)$$

$$\bar{\mu} = \frac{1}{2d} \int_0^d dz_1 \int_0^\pi \sin \theta_1 d\theta_1 \cos(\frac{2\pi z_1}{d}) \exp[sum] \quad (2.15)$$

$$\tau = \frac{1}{2d} \int_0^d dz_1 \int_0^\pi \sin \theta_1 d\theta_1 P_2(\cos \theta_1) \cos(\frac{2\pi z_1}{d}) \times \exp[sum] \quad (2.16)$$

and change in density at the transition is found from the relation

$$1 + \Delta\rho^* = \frac{1}{2d} \int_0^d dz_1 \int_0^\pi \sin\theta_1 d\theta_1 \exp[sum]. \quad (2.17)$$

Here

$$\begin{aligned} sum = & \Delta\rho^* \hat{C}_{00}^0 + 2\bar{\mu} \cos\left(\frac{2\pi z_1}{d}\right) \hat{C}_{00}^1(\theta_1) + \bar{P}_2 \hat{C}_{20}^0(\theta_1) + \\ & \bar{P}_4 \hat{C}_{40}^0(\theta_1) + 2\tau \cos\left(\frac{2\pi z_1}{d}\right) \hat{C}_{20}^1(\theta_1) \end{aligned} \quad (2.18)$$

and

$$\begin{aligned} \hat{C}_{L0}^q(\theta_1) = & \left(\frac{2l+1}{4\pi}\right)^{1/2} \rho_f \sum_{l_1 l} i^l (2l_1+1)^{1/2} (2l+1)^{1/2} \times \\ & P_{l_1}(\cos\theta_1) C_g(l_1 L l; 000) \times \\ & \int_0^\infty c_{l_1 L l}(r_{12}) j_l(G_q r_{12}) r_{12}^2 dr_{12} \end{aligned} \quad (2.19)$$

where $c_{l_1 L l}(r)$ are direct pair correlation function harmonics, $C_g(l_1 L l; 000)$ are Clebsch-Gordan coefficients and $G_q = 2\pi/d$.

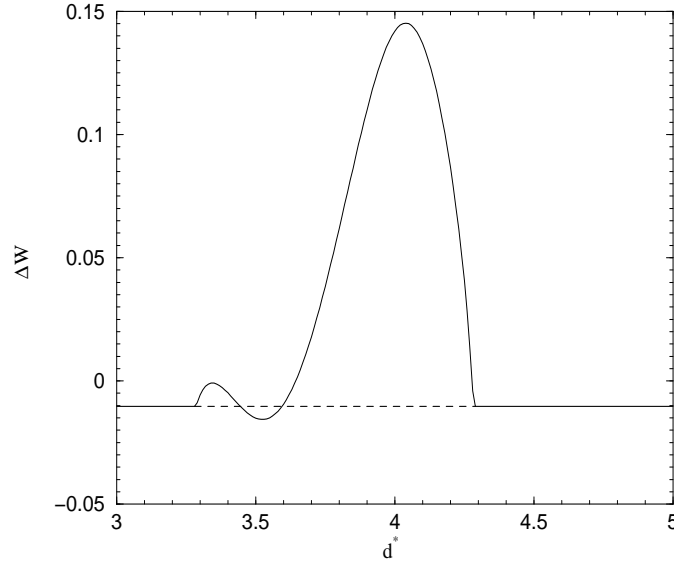


FIG. 1: Variation of grand thermodynamic potential with smectic interlayer spacing for nematic-smectic A transition density $\rho^* = 0.219$ at $T^* = 1.40$ for the GB potential parameters $x_0 = 4.0$, $k' = 5$, $\mu = 2$ and $\nu = 1$.

In order to evaluate the transition parameters such as order parameters, change in density etc, equation (15)-(21) were solved self consistently using values of the harmonics $c_{l_1 L l}(r)$

evaluated at given temperature and density for each value of x_0 . The calculation is repeated with different values of Sm A interlayer spacing, d . By substituting these solutions in Equations (7)-(9) we find the grand thermodynamic potential difference between ordered and isotropic phases; i.e.

$$-\frac{\Delta W}{N} = -\Delta\rho^* + \frac{1}{2}\Delta\rho^*(2 + \Delta\rho^*)\hat{C}_{00}^0 + \frac{1}{2}(\bar{P}_2^2\hat{C}_{22}^0 + \bar{P}_4^2\hat{C}_{44}^0) + \bar{\mu}^2\hat{C}_{00}^1 + 2\bar{\mu}\tau\hat{C}_{20}^1 + \tau^2\hat{C}_{22}^1 \quad (2.20)$$

where

$$\begin{aligned} \hat{C}_{LL'}^q = & (2L+1)^{1/2}(2L'+1)^{1/2} \times \\ & \rho_f \sum_l i^l \left(\frac{2l+1}{4\pi}\right)^{1/2} C_g(LL'l; 000) \times \\ & \int_0^\infty c_{LL'l}(r_{12}) j_l(G_q r_{12}) r_{12}^2 dr_{12} \end{aligned} \quad (2.21)$$

At given temperature and density the phase with lowest grand potential is taken as the stable phase. Phase coexistence occurs at the value of ρ_f that makes $-\Delta W/N = 0$ for the ordered and the liquid phases. The transition from nematic to the SmA is determined by comparing the values of $-\Delta W/N$ of these two phases at a given temperature and at different densities. The value of the interlayer spacing d , is found by minimizing the grand potential with respect to d . In Fig.1 we plot the variation of ΔW with $d^*(= d/\sigma_0)$. After selecting the value of d for a given density and temperature we locate the transition point using the procedure outlined above. In the isotropic phase all the four order parameters become zero. In the nematic phase the orientational order parameters \bar{P}_2 and \bar{P}_4 become nonzero but the other two parameters $\bar{\mu}$ and τ remain zero. This is because the nematic phase has no long range positional order. In the SmA phase all the four order parameters are nonzero showing that the system has both long range orientational and positional order along one direction.

III. RESULTS AND DISCUSSION

The pair correlation functions(PCF's) of molecular fluids are the lowest order microscopic quantities which contain information about the structure of the fluid as well as have direct contact with the underlying intermolecular interactions. Most of the structural informations of an ordered phase are contained in single particle distribution $\rho(x)$, as shown in the previous

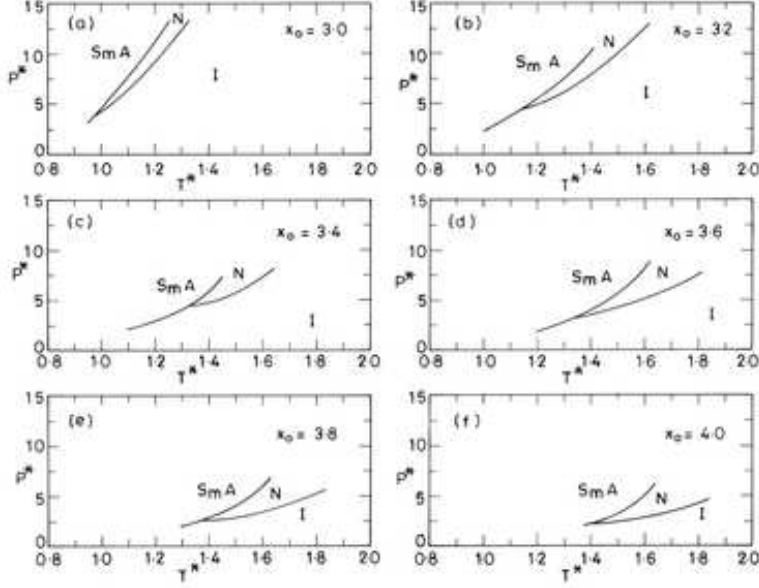


FIG. 2: Pressure-Temperature phase diagrams for the GB potential with parameters $3.0 \leq x_0 \leq 4.0$, $k' = 5$, $\mu = 2$ and $\nu = 1$ using density-functional theory

section. In the DFT of freezing the single particle distribution $\rho(x)$ of an ordered phase is expressed in terms of the PCF's of the isotropic fluid. In this study, the PCF's of the isotropic phase are found by solving Ornstein-Zernike (OZ) equation using Percus-Yevick (PY) closure (details are same as in reference [18]) at different values of the reduced temperatures T^* , in the range from 0.80 to 1.80 and at various densities for each $3.0 \leq x_0 \leq 4.0$.

In Figures 2(a-f) we present the phase diagrams in the pressure-temperature plane. For all $x_0 \geq 3.0$, we first find the direct I-Sm A transition below a certain temperature T^* which increases from $T^* \simeq 0.99$ for $x_0 = 3.0$ to $T^* \simeq 1.39$ for $x_0 = 4.0$. The lowest temperature where Sm A phase starts stabilizing is found to rise as we increase x_0 . On further increase in T^* , nematic phase enters into the phase sequence. Temperature range of nematic stability is found to increase as molecular elongation is increased which is also reflected in the ratio of N-Sm A and I-N transition temperatures, T_{N-A}/T_{I-N} . For example, the value of the ratio change from 0.96 to 0.92 as we move from $x_0 = 3.6$ to $x_0 = 4.0$ with pressure, P^* , fixed at 3.5. This corresponds to a higher orientational order before the Sm A phase stabilizes. According to McMillan theory [20], this value of the T_{N-A}/T_{I-N} ratio predicts that the N-Sm A transition is first order. Figs. 2(a-f) also show that as x_0 is increased, both the I-N and N-Sm A transitions move to a lower pressure.

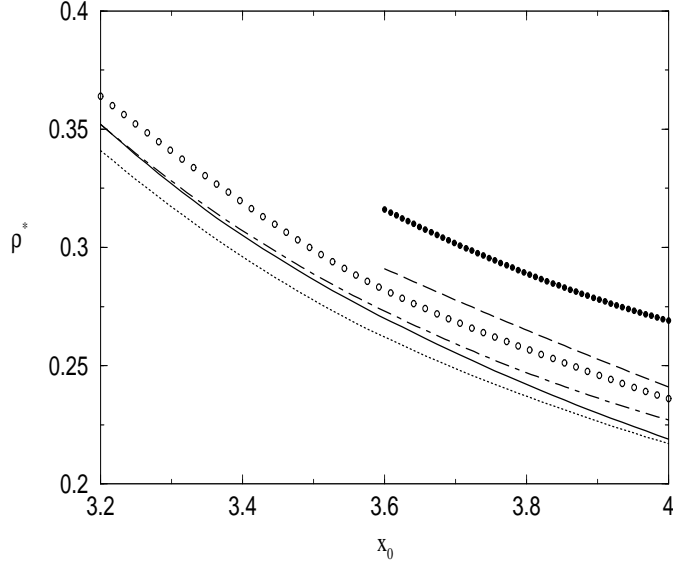


FIG. 3: Variation of I-N and N-Sm A transition densities with molecular elongation parameter x_0 . Dotted and solid lines represent, respectively, I-N and N-Sm A transition densities at $T^* = 1.40$. Dot-dashed and long dashed lines are the respective lines at $T^* = 1.50$ and open circles and filled circles are those at $T^* = 1.60$, respectively.

In Figures 3, we plot the I-N and N-Sm A transition densities against the molecular elongation x_0 . Both the I-N and N-Sm A transition densities are seen to decrease with the increase in x_0 in agreement to reference [9]. It can be seen from this figure that the difference between the I-N and N-Sm A transition densities decreases as x_0 is increased. This is more apparent in the low temperature curves where the region between the two transition lines gradually shrinks. This makes evident that for a given temperature, with the increase in molecular elongation, the Sm A phase become more probable at low density and eventually takes over nematic resulting in direct isotropic to Sm A transition. This stabilization of smectic phase is to be expected since increase in x_0 results in deeper well depth for parallel configuration of molecules making it energetically more favourable. Also the I-N and N-Sm A transition density difference is seen to decrease rapidly as the temperature is reduced at a fixed x_0 , showing the effect of the attractive intermolecular interaction which dominates at low temperature facilitating the formation of the Sm A Phase. This also indicates the possibility of direct I- Sm A transition for a given x_0 below certain temperature where Sm A phase takes over nematic.

The Sm A phase is characterized by the presence of a non zero translational and mixed

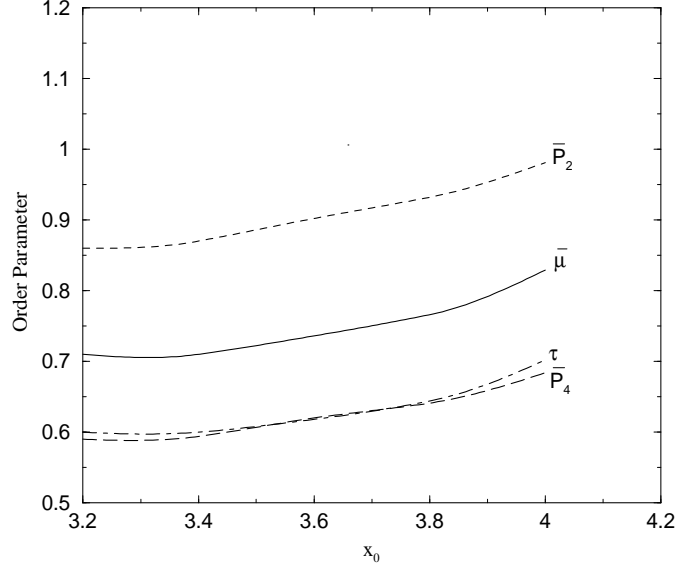


FIG. 4: Variation of order parameters with x_0 for N-Sm A transition at $T^* = 1.40$ keeping other GB potential parameters fixed at $k' = 5, \mu = 2$ and $\nu = 1$.

order parameters along with the orientational order parameters. Fig.4 presents the variation of the order parameters at N-Sm A transition with respect to x_0 at temperature (arbitrarily chosen) $T^* = 1.40$. It shows that the order parameters are monotonically increasing with the increase in the molecular elongation. For each x_0 , we found that the values of translational and mixed order parameters, which are characteristics of Sm A phase, decrease rapidly with the increase in temperature, eventually becoming zero. This shows that the stable Sm A phase becomes progressively less ordered with the increasing temperature and finally destabilizes with respect to nematic phase and disappears from the phase diagram. This is obvious as attractive forces between the molecules are less important at high temperatures and purely repulsive intermolecular interactions do not exhibit Sm A. One should note that at $x_0 = 3.0$, we get stable Sm A phase which has not been observed in computer simulation experiments. The phase observed in simulation [9] is Sm B which we have not considered in the present study. In Table 1 we have compared our results for the I-N transition parameters with the simulation results of refs.[12, 13] at temperature $T^* = 1.00$ for $x_0 = 3.0$. It can be seen that the values of the transition parameters found by us are higher than those of the simulations but relatively close to the values of ref.[13].

The change in density at transitions $\Delta\rho^*(= \frac{\rho_n - \rho_l}{\rho_l})$ is found to increase as x_0 is increased at a given temperature. For example, for $T^* = 1.50$, at I-N transition $\Delta\rho^*$ changes from

TABLE I: Comparison of isotropic-nematic transition parameters of the GB(3, 5, 2, 1) potential at $T^* = 1.00$. Quantities in reduced units are Pressure $P^* = P\sigma_0^3/\epsilon_0$, and $\mu_c^* = \mu_c/\epsilon_0$.

Theory	ρ^*	$\Delta\rho^*$	\bar{P}_2	\bar{P}_4	P^*	μ_c^*
DFT	0.336	0.017	0.675	0.373	4.41	14.57
MC[13]	0.320	-	0.660	0.290	-	-
MC[12]	0.307	0.017	0.520	-	3.63	12.79

4.9% to 6.0% as x_0 is changed from 3.8 to 4.0, whereas the corresponding change at the N-Sm A transition is from 3.4% to 4.7%. In the simulation [9], though the value of $\Delta\rho^*$ at the N-Sm A transition increases from $\sim 1.6\%$ to $\sim 3.1\%$ as x_0 changes from 3.8 to 4.0, the trend at I-N transition is reverse where it decreases from $\sim 8\%$ to $\sim 5.2\%$.

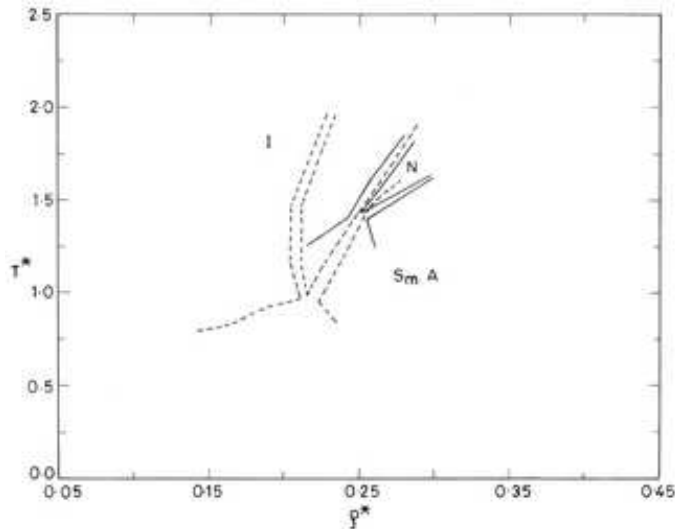


FIG. 5: Temperature-Density phase diagram for the GB potential with parameters $x_0 = 3.8, k' = 5, \mu = 2$ and $\nu = 1$. The solid lines indicate the phase boundaries obtained by using the density-functional theory while dashed lines are the simulation results of Brown *et al*[9].

In Figs. 5 and 6 we present our phase diagram in the temperature-density plane for $x_0 = 3.8$ and 4.0. The solid lines represent the phase boundaries calculated by us while dashed lines are the approximate phase boundaries taken from ref. [9] for the sake of comparison. Though the quantitative agreement between the phase diagrams shown in the Figures 5 and 6 is not so encouraging, however, they agree qualitatively well. This may be due to the fact that in our calculation the transition takes place at higher density

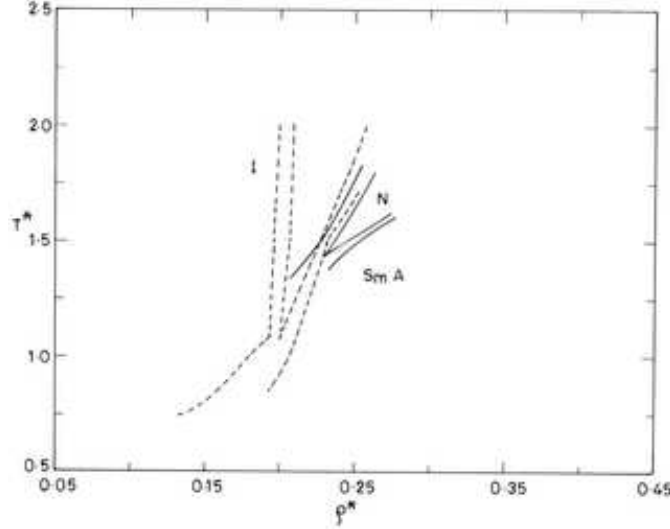


FIG. 6: Temperature-density phase diagram for the GB potential with parameters $x_0 = 4.0$, $k' = 5$, $\mu = 2$ and $\nu = 1$. The curves are the same as in figure 5.

than those found in the simulations. The critical correlations at which the isotropic phase become unstable are found to be higher than actual values because PY theory is known to underestimate the orientational correlations[21]. This shortcoming of the PY theory is found to increase with increasing temperature which explains why in Figs. 5 and 6 the I-N transition boundaries are more shifted than the N-Sm A boundaries.

IV. CONCLUSION

We have used the Gay-Berne potential model, to study the effect of the variation of elongation parameter x_0 on its phase behaviour with the values of all other parameters fixed at $k' = 5$, $\mu = 2$ and $\nu = 1$. The pair correlation functions of the isotropic fluid are calculated using Percus-Yevick integral equation theory and have been used in density-functional theory to locate the isotropic-nematic, isotropic-smectic A and nematic-smectic A transitions. Within the small range of elongation $3.0 \leq x_0 \leq 4.0$, the phase diagram shows significant changes. We have discussed how various phase boundaries, transition densities, pressure, change in density at transition, order parameters etc. change with the variation in molecular elongation. We found a stable Sm A phase for all $x_0 \geq 3.0$. Both I-N and N-Sm A transitions are found to move to lower density and pressure as x_0 is increased. We have compared our results with those of computer simulations and found

that the density-functional theory reproduces all the features of the phase diagrams which are in good qualitative agreement. To have a better quantitative agreement there is a need to evaluate the isotropic pair correlations more accurately than those given by Percus-Yevick theory. Also the use of correlations evaluated directly in the nematic phase may improve the results. The work in this direction is in progress.

V. ACKNOWLEDGMENT

We are grateful to Prof. Y. Singh for many helpful discussions and encouragement. The work was supported by Department of Science and Technology (India) through a project grant.

-
- [1] P.G de Gennes and J. Prost, *The Physics of Liquid Crystals*, (Clarendon, Oxford, 1993); S Chandrasekhar *Liquid Crystals*, (Cambridge University Press,London, 1977)
 - [2] J. G. Gay and B. J. Berne, J. Chem Phys. **74**, 3316 (1981)
 - [3] G. R. Luckhurst and P. S. J Simmonds, Mol. Phys. **80**, 233 (1993)
 - [4] E. de Miguel, L. F. Rull, M. K. Chalam, K. E. Gubbins and E. V. Swol, Mol. Phys. **72**, 593 (1991)
 - [5] E. de Miguel, L. F. Rull, M. K. Chalam and K. E. Gubbins, Mol. Phys. **74**, 405 (1991)
 - [6] G. R. Luckhurst, R. A. Stephens and R. W. Phippen, Liq. Cryst. **8**, 451 (1990)
 - [7] E. de Miguel, E. Martin del Rio, J. T.Brown and M. P. Allen, J. Chem. Phys. **105**, 4234 (1996)
 - [8] M. P. Allen, J. T. Brown and M. A. Warren, J. Phys.: Condens. Matter **8**, 9433 (1996)
 - [9] J. T. Brown, M. P. Allen and E. Martin del Rio, and E. de Miguel, Phys. Rev. E **57**, 6685 (1998)
 - [10] M. A. Bates and G. R. Luckhurst, J. Chem. Phys. **110**, 7087 (1999)
 - [11] E. de Miguel and E. Martin del Rio, J. Chem. Phys. **118**, 1852 (2003)
 - [12] E. de Miguel, Molec. Phys **100**, 2449 (2002)
 - [13] L. Longa, G. Cholewiak, R. Terbin and G. R. Luckhurst, Eur. Phys. J. E **4**, 51 (2001)
 - [14] E. Velasco, A. M. Somoza and L. Mederos, J. Chem. Phys.**102**, 8107 (1995)

- [15] E. Velasco and L. Mederos, J. Chem. Phys. **109**, 2361 (1998)
- [16] R. C. Singh, J. Ram and Y. Singh, Phys. Rev. E **65**, 031711 (2002)
- [17] R. C. Singh and J. Ram , Physica A **326**, 13 (2003)
- [18] P. Mishra, J. Ram and Y. Singh, J. Phys.: Condens. Matter **16**, 1695 (2004)
- [19] Y. Singh, Phys. Rep. **207**, 351 (1991)
- [20] W. L. McMillan, Phys. Rev. A **4**, 1238 (1971)
- [21] R. C. Singh, J. Ram and Y. Singh, Phys. Rev. E **54**, 977 (1996); S. Singh, Phys. Rep. **324**, 107 (2000)